OXFORD

Human Molecular Genetics, 2016, Vol. 25, No. 19 4244–4255

doi: 10.1093/hmg/ddw256
Advance Access Publication Date: 11 August 2016
Original Article

ORIGINAL ARTICLE

Reprogramming towards anabolism impedes degeneration in a preclinical model of retinitis pigmentosa

Lijuan Zhang[1,2,3], Sally Justus[1,2], Yu Xu[1,2,4], Tamara Pluchenik[1,2], Chun-Wei Hsu[1,2], Jin Yang[1,2,5], Jimmy K. Duong[6], Chyuan-Sheng Lin[7], Yading Jia[3], Alexander G. Bassuk[8], Vinit B. Mahajan[9,10] and Stephen H. Tsang[1,2,*]

[1]Barbara & Donald Jonas Stem Cell & Regenerative Medicine Laboratory, and Bernard & Shirlee Brown Glaucoma Laboratory, Departments of Ophthalmology and Pathology & Cell Biology, Institute of Human Nutrition, Herbert Irving Comprehensive Cancer Center, Columbia University, New York, NY, USA, [2]Edward S. Harkness Eye Institute, New York-Presbyterian Hospital, New York, NY, USA, [3]Shanxi Eye Hospital, affiliated with Shanxi Medical University, Xinghualing, Taiyuan, Shanxi, China, [4]Department of Ophthalmology, Xinhua Hospital Affiliated to Shanghai Jiao Tong University School of Medicine, Shanghai, China, [5]Tianjin Medical University Eye Hospital, Tianjin, China, [6]Department of Biostatistics, Mailman School of Public Health, Columbia University Medical Center, New York, USA, [7]Department of Pathology and Cell Biology, Transgenic Animal Facility, Herbert Irving Comprehensive Cancer Center, College of Physicians and Surgeons of Columbia University, New York, NY, USA, [8]Department of Pediatrics and Neurology, University of Iowa, Iowa City, IA, [9]Omics Laboratory, University of Iowa, Iowa City, IA, USA and [10]Department of Ophthalmology and Visual Sciences, University of Iowa, Iowa City, IA, USA

*To whom correspondence should be addressed at: Stephen H. Tsang, Edward S. Harkness Eye Institute, New York-Presbyterian Hospital/Columbia University Medical Center, 635 West 165th Street, Box 112, New York, NY 10032, USA. Tel: 212-342-1186; Fax: 212-305-4987; Email: sht2@columbia.edu

Abstract

Retinitis pigmentosa (RP) is an incurable neurodegenerative condition featuring photoreceptor death that leads to blindness. Currently, there is no approved therapeutic for photoreceptor degenerative conditions like RP and atrophic age-related macular degeneration (AMD). Although there are promising results in human gene therapy, RP is a genetically diverse disorder, such that gene-specific therapies would be practical in a small fraction of patients with RP. Here, we explore a non-gene-specific strategy that entails reprogramming photoreceptors towards anabolism by upregulating the mechanistic target of rapamycin (mTOR) pathway. We conditionally ablated the tuberous sclerosis complex 1 (*Tsc1*) gene, an mTOR inhibitor, in the rods of the *Pde6b*$^{H620Q/H620Q}$ preclinical RP mouse model and observed, functionally and morphologically, an improvement in the survival of rods and cones at early and late disease stages. These results elucidate the ability of reprogramming the metabolome to slow photoreceptor degeneration. This strategy may also be applicable to a wider range of neurodegenerative diseases, as enhancement of nutrient uptake is not gene-specific and is implicated in multiple pathologies. Enhancing

Received: April 26, 2016. **Revised:** June 25, 2016. **Accepted:** July 22, 2016

anabolism promoted neuronal survival and function and could potentially benefit a number of photoreceptor and other degenerative conditions.

Introduction

Retinitis pigmentosa (RP) is an incurable neurodegenerative condition that leads to progressive photoreceptor dysfunction, dysmorphosis and symptoms such as nyctalopia, tunnel vision and eventually, blindness (1–4). This disease is estimated to affect nearly 1 million people worldwide and leads to a substantial decrease in the ability of affected individuals to lead independent lives and conduct activities of daily living (1,2). A heterogeneous genetic condition, RP is linked to more than 60 genes, most of which occur in genes that are exclusively expressed in rod photoreceptors (5–7). Due to the genetic diversity of RP, any therapy that is gene specific can only benefit a small fraction of patients with RP. There is currently no effective therapeutic option for patients with RP or any other patient with a retinal degenerative disease, including atrophic age-related macular degeneration (AMD), which affects more than 1.5 million individuals in the United States (8).

In RP, mutations in genes encoding phototransduction enzymes such as rhodopsin and phosphodiesterase 6 (PDE6) impair photoexcitation, creating imbalance between anabolic and catabolic processes that leads to shortening of the outer segments (OS) of photoreceptors and eventually triggering cell death (2,9–12). The OS is shed and regenerated daily, but in diseased photoreceptors, there are aberrations in the renewal cycle that lead to significantly shorter OS and subsequent dysgenesis (2,9). Augmenting anabolism could theoretically fuel protein and lipid synthesis, thus encouraging OS regenesis. This strategy could potentially serve as a treatment for RP by reprogramming rods towards anabolism, preserving their ability to maintain the OS, and increasing their chance of survival.

The mechanistic target of rapamycin (mTOR) pathway has been identified as a key regulator of anabolism, including such pathways as cellular metabolism and growth based on cues such as stress, hypoxia, growth factors and glucose concentration (13–15). Binding of growth factors like insulin activates the mTOR complex (mTORC), promoting anabolic processes such as ribosome biogenesis, protein synthesis and transcription (16,17). Simultaneously, catabolic processes like autophagy and apoptosis are suppressed (18,19). A similar effect is achieved in the presence of high levels of amino acids and nutrients. Previously, we collected preliminary data on the effects of mTOR upregulation by shRNA-mediated silencing of the tuberous sclerosis complex 2 (TSC2) in a mouse model of RP and found increased photoreceptor numbers and preservation of function (20). Similar results were obtained by Punzo et al. when the mTOR pathway was upregulated in cones in four different mouse models of RP (21).

In this paper, we expand on previous findings by exploring the effects of a specific ablation of *Tsc1* in rods, which has not been explored before, using a tamoxifen-inducible, rod-specific *Tsc1* knockout $Pde6b^{H620Q/H620Q}$ RP model. The $Pde6b^{H620Q/H620Q}$ mutation prevents normal activation of the phototransduction cascade and features rod OS dysgenesis (20,22). While heterozygous mice are phenotypically normal, homozygotes experience relatively rapid photoreceptor degeneration (20,22). We hypothesize that upregulation of mTOR in rods by *Tsc1* knockout can facilitate both rod and cone morphological and functional preservation and enhanced survival.

Results

Effects of TSC1 deficiency in $Pde6b^{H620Q/+}$ heterozygotes

To determine whether *Tsc1* knockout in phenotypically wild type mice affects retina morphology or function, we generated a tamoxifen-inducible, rod-specific Cre recombinase mouse line by crossing $Tsc1^{tm1Djk/J}$, $Pde6b^{H620Q/+}$ and $Pde6g^{CreERT2}$ mice. Following intraperitoneal (IP) injection of tamoxifen, exons 17 and 18 of the *Tsc1* gene was excised, leaving the mice with a nonfunctional *Tsc1* protein, one functional copy of *Pde6b*, and the genotype, $Tsc1^{-/-}Pde6b^{H620Q/+}Pde6g^{CreERT2}$. Control mice were injected with oil instead of tamoxifen and thus had the genotype, $Tsc1^{loxP/loxP}Pde6b^{H620Q/+}Pde6g^{CreERT2}$. Five weeks following injection, electroretinogram (ERG) recordings of scotopic, photopic and mixed rod-cone magnitudes were acquired and revealed no statistically significant difference between the groups (Fig. 1A–C). Retinae were harvested and exposed to H&E staining at 6 weeks, revealing comparable morphology of the outer nuclear layer (ONL), inner segment (IS) and OS in the control and experimental groups' retinae (Fig. 1A). These findings suggest that Cre induction and *Tsc1* knockout do not affect the function or morphology of wild type mouse retinae.

Anatomical rescue in $Pde6b^{H620Q/H620Q}$ homozygotes lacking TSC1 at early and late stages

Subsequently, a second line of tamoxifen-inducible *Tsc1* knockout mouse was generated that was homozygous at the *Pde6b* locus for the H620Q point mutation. Following tamoxifen injection, the experimental group, hereafter referred to as treated, experimental, knockout, or $Tsc1^{-/-}Pde6b^{H620Q/H620Q}$, had a complete ablation of *Tsc1* in rods, while the control group, denoted control or $Tsc1^{loxP/loxP}Pde6b^{H620Q/H620Q}$, had normal *Tsc1* expression. Histology was performed weekly and revealed a more robust and healthy ONL in $Tsc1^{-/-}Pde6b^{H620Q/H620Q}$ at early time points (before postnatal 3 weeks) compared to $Tsc1^{loxP/loxP}Pde6b^{H620Q/H620Q}$ mice as measured by ONL nuclei density and width (Fig. 2). ONL cell density and thickness were statistically greater in the experimental group at 1 and 2 weeks after injection compared to controls, although in both groups, a decrease was observed over time. Conversely, the IS/OS layer width increased over time, as would be expected according to physiological photoreceptor development (23,24). Notably, the $Tsc1^{-/-}Pde6b^{H620Q/H620Q}$ mice IS/OS layer width was thicker at each time point compared to that of the control mice (Fig. 2B). The predicted trend line for the ONL nuclei density and width was negative for both groups but steeper for the control group. Conversely, the predicted trend line was positive and steeper for the IS/OS layer thickness in the $Tsc1^{-/-}Pde6b^{H620Q/H620Q}$ experimental mice compared to controls. However, this rescue diminished over time (Fig. 3). Histology revealed decreasing thickness in both groups' ONL and IS/OS layers at later time points, although the width of the layers in the knockout mice remained noticeably thicker even at the final time point (Fig. 3). Unexpectedly, trend lines mapping ONL nuclei density and width were steeper in the treated group compared to the control mice, which opposes findings obtained in the early stages following IP injection (Fig. 3B). Another distinguishing

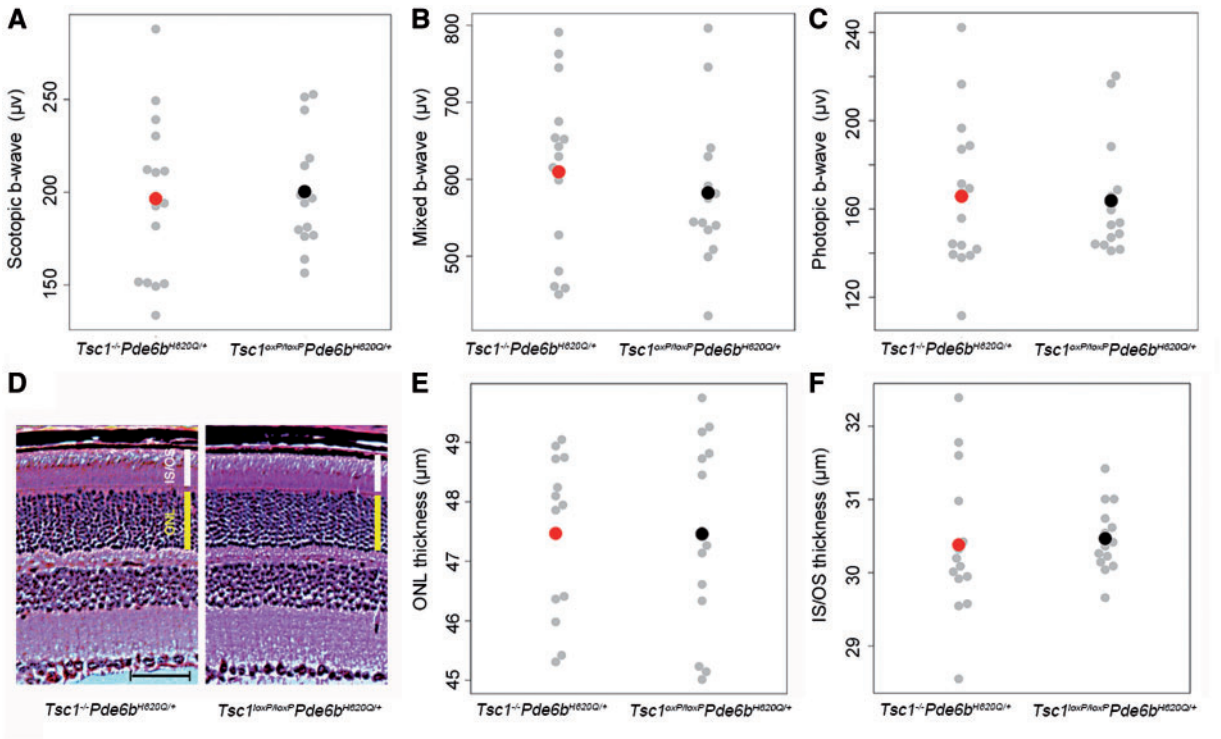

Figure 1. ERG b-wave magnitudes and histology are comparable in $Tsc1^{-/-}Pde6b^{H620Q/+}$ and $Tsc1^{loxP/loxP}Pde6b^{H620Q/+}$ mice. **(A-C)** Scotopic, mixed maximal, and photopic ERG recordings were acquired at 5 weeks post injection. Small grey dots represent data points from eyes; bold red dots represent means for the $Tsc1^{-/-}Pde6b^{H620Q/+}$ mice, and bold black dots represent means for the $Tsc1^{loxP/loxP}Pde6b^{H620Q/+}$ mice. To compare mean ERG outcomes or mean histological outcomes between the $Tsc1^{-/-}Pde6b^{H620Q/+}$ and $Tsc1^{loxP/loxP}Pde6b^{H620Q/+}$ groups, linear mixed models with random intercepts for mice were fit. Average b-wave magnitudes between the groups had no statistically significant mean difference. ((A) $P = 0.80$; (B) $P = 0.59$; (C) $P = 0.89$). **(D-F)** H&E staining of retinal sections also had comparable mean ONL and IS/OS layers between the groups. These values were quantified by measuring the thickness of the ONL and IS/OS, which were observed to be statistically insignificant. ((D) Yellow bar indicates ONL, white bar indicates IS/OS, scale bar = 50 μm; (E) $P = 0.98$ (F) $P = 0.78$; for ERG, $n = 8$ for $Tsc1^{-/-}Pde6b^{H620Q/+}$, $n = 7$ for $Tsc1^{loxP/loxP}Pde6b^{H620Q/+}$; for histology, $n = 7$ for both groups.).

characteristic of the late stage (4–10 weeks) compared with the early stage is that the IS/OS layer thickness diminished over time in both groups, while in the early stage it increased with time. The predicted trend line between the groups was parallel, although the $Tsc1^{-/-}Pde6b^{H620Q/H620Q}$ group had an overall higher mean thickness at each time point.

Functional rescue of photoreceptors in $Pde6b^{H620Q/H620Q}$ homozygotes lacking TSC1

Functional assay of photoreceptor vitality was determined by scotopic, photopic and mixed ERG recordings at biweekly intervals from 4 to 12 weeks (Fig. 4A). A decline in the recording amplitudes over time was evident even in the experimental group, but the average magnitude of scotopic, photopic and mixed ERG recordings was statistically higher at every time point in $Tsc1^{-/-}Pde6b^{H620Q/H620Q}$ compared to $Tsc1^{loxP/loxP}Pde6b^{H620Q/H620Q}$ mice. By 12 weeks, the ERG was no longer detectable in the control mice, while the experimental group still retained a low but measurable b-wave magnitude. Scotopic and mixed b-wave data were acquired under dark-adapted conditions to measure rod and maximal rod-cone responses, respectively, while photopic data were acquired under light-adapted conditions to trigger the cone response (Fig. 4B). All conditions exhibited a statistically greater b-wave amplitude in the $Tsc1^{-/-}Pde6b^{H620Q/H620Q}$ group compared to the control group at all time points. There was a decrease in statistical significance over time that may have been due to the loss of rods early on, leading to diminished differences between the control and experimental ERG recordings at later time points.

Robust immunoreactivity of rhodopsin in rods and cone arrestin in the cones of $Tsc1^{-/-}Pde6b^{H620Q/H620Q}$ mice

Rhodopsin (RHO) is a rod-specific protein essential to the phototransduction pathway, and expression levels of this protein are correlated with functional capability in phototransduction. Retinal sections were immunostained for RHO at multiple time points (Fig. 5A), revealing stronger expression in the $Tsc1^{-/-}Pde6b^{H620Q/H620Q}$ mice than in the $Tsc1^{loxP/loxP}Pde6b^{H620Q/H620Q}$ mice at every time point. In both groups, there was a gradual decline in protein expression over time, although by 12 weeks, RHO staining was scarcely observed in the $Tsc1^{loxP/loxP}Pde6b^{H620Q/H620Q}$ mouse while it persisted in the $Tsc1^{-/-}Pde6b^{H620Q/H620Q}$ group. RHO expression was quantified by measuring the width of cells expressing the protein and was found to corroborate the imaging data (Fig. 5B). Sections were also stained for cone arrestin, which is a cone-specific G protein-coupled receptor (GPCR) modulator (Fig. 6A). While $Tsc1^{-/-}Pde6b^{H620Q/H620Q}$ mice showed more robust expression than $Tsc1^{loxP/loxP}Pde6b^{H620Q/H620Q}$ mice at every time point, there was a gradual decline in cone arrestin expression in both groups over time. By 20 weeks, cone arrestin was no longer detectable in the control group, while some indications of its presence

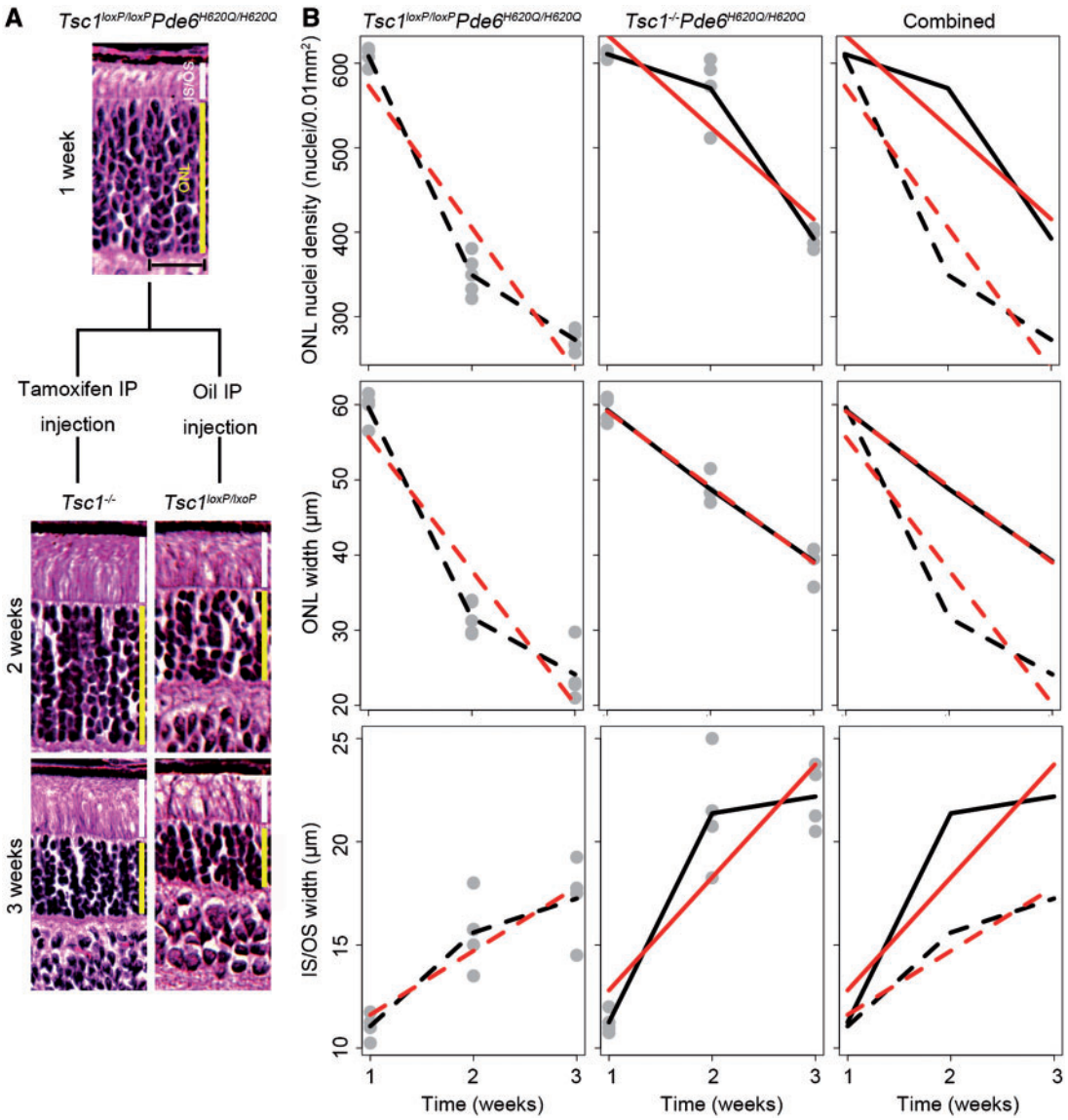

Figure 2. *Tsc1*$^{-/-}$*Pde6b*$^{H620Q/H620Q}$ have enhanced photoreceptor survival compared to *Tsc1*$^{loxP/loxP}$*Pde6b*$^{H620Q/H620Q}$ controls for at least 3 weeks. **(A)** H&E-stained retinal sections were compared at 10, 17, and 24 days. ONL and IS/OS thickness were greater at every time point in the *Tsc1*$^{-/-}$*Pde6b*$^{H620Q/H620Q}$ group compared to controls. Tamoxifen or oil injection occurred at P10. Histology was quantified statistically over time. (Yellow bar indicates ONL, white bar indicates IS/OS, scale bar = 20 μm.). **(B)** ONL nuclei density and ONL layer width were greater in *Tsc1*$^{-/-}$*Pde6b*$^{H620Q/H620Q}$ mice compared to *Tsc1*$^{loxP/loxP}$*Pde6b*$^{H620Q/H620Q}$ mice at every time point. IS/OS width was quantified and observed to increase over time in both groups, although the *Tsc1*$^{-/-}$*Pde6b*$^{H620Q/H620Q}$ group had a greater mean thickness at each time point compared to the controls. Predicted trend lines for the ONL had steeper slopes for the control mice compared to the experimental group for both nuclei density and layer thickness. IS/OS trend lines were positively sloped and steeper for the experimental group compared to controls. (Grey dots represent individual mouse data points. Black lines connect the mean outcome at each time point; red lines are estimated mean trend lines from linear regression models, assuming linearity of the outcome over time. Dashed lines are used for controls, and solid lines are used for knockout mice. Comparisons of *Tsc1*$^{-/-}$*Pde6b*$^{H620Q/H620Q}$ versus *Tsc1*$^{loxP/loxP}$*Pde6b*$^{H620Q/H620Q}$ controls at fixed points: ONL nuclei density: P17 $P < 0.001$, P24 $P < 0.001$; ONL width: P17 $P < 0.001$; P24 $P = 0.001$. IS/OS width: P17 $P = 0.02$, P24 $P = 0.009$. Comparison of the slopes between the two groups from the linear regression models: ONL density: $P = 0.02$, ONL width $P = 0.003$, IS/OS $P = 0.06$. P10 $n = 4$ for both groups, P17 and P24 $n = 5$ for *Tsc1*$^{-/-}$*Pde6b*$^{H620Q/H620Q}$ and $n = 4$ for *Tsc1*$^{loxP/loxP}$*Pde6b*$^{H620Q/H620Q}$).

were observable in the *Tsc1*$^{-/-}$*Pde6b*$^{H620Q/H620Q}$ mice. Cone density was quantified by counting cell nuclei and was found to be greater in the *Tsc1*$^{-/-}$*Pde6b*$^{H620Q/H620Q}$ group at all time points compared to controls (Fig. 6B).

Downstream targets of mTOR were upregulated in *Pde6b*$^{H620Q/H620Q}$ homozygotes lacking TSC1

Phosphorylation of the mTOR proteins was assessed by immunofluorescence staining at P21 and revealed heightened expression in the experimental group compared to the control group (Fig. 7A). Individual segments of the IS/OS tips were clearly delineated in *Tsc1*$^{-/-}$*Pde6b*$^{H620Q/H620Q}$ when stained for phosphorylated mTOR (p-mTOR), while they were indistinguishable in the *Tsc1*$^{loxP/loxP}$*Pde6b*$^{H620Q/H620Q}$ controls. A downstream target of this pathway, phospho-S6 (pS6), was also stained and found to be greater in the *Tsc1*$^{-/-}$*Pde6b*$^{H620Q/H620Q}$ mice. Immunoblot revealed a significantly less intense TSC1 band in the knockout mice compared to the controls, which likely arose from *Tsc1* expression in cones, bipolar cells and

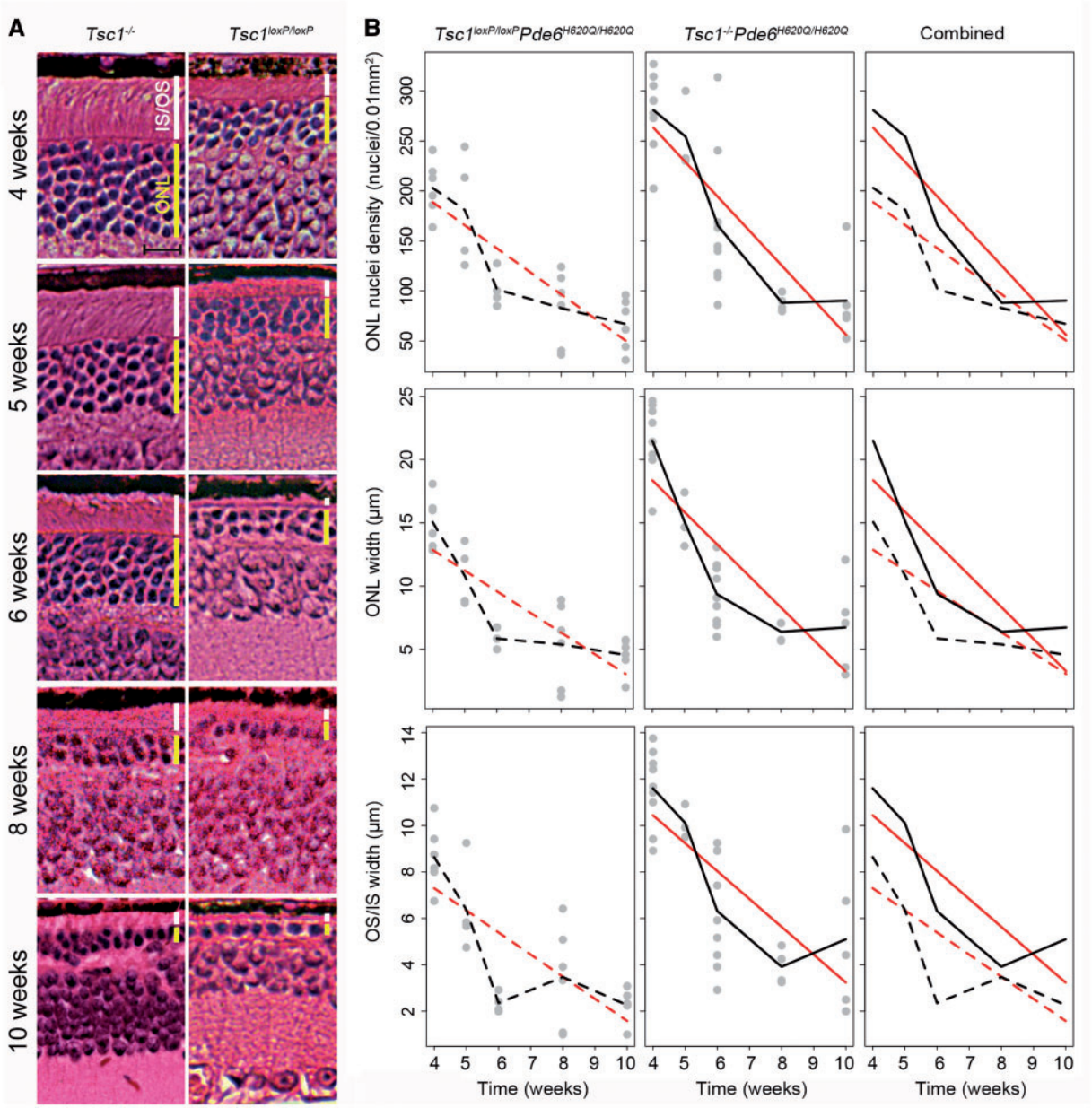

Figure 3. *Tsc1*$^{-/-}$*Pde6b*$^{H620Q/H620Q}$ have improved retinal survival compared to *Tsc1*$^{loxP/loxP}$*Pde6b*$^{H620Q/H620Q}$ controls for at least 10 weeks. **(A)** H&E-stained retinal sections were compared at 4, 5, 6, 8, and 10 weeks. Mean ONL and IS/OS thickness were greater at every time point in the *Tsc1*$^{-/-}$*Pde6b*$^{H620Q/H620Q}$ group, compared to controls. (Yellow bar indicates ONL, white bar indicates IS/OS, scale bar = 20 μm.) **(B)** This difference was quantified by counting ONL nuclei density and measuring the width of the ONL and IS/OS over time. *Tsc1*$^{-/-}$*Pde6b*$^{H620Q/H620Q}$ mice had higher mean nuclei numbers and mean layer width in the ONL and IS/OS at all-time points compared to controls, although the differences between the groups diminished over time. The predicted trend line for the ONL nuclei density and width was negative for both groups but steeper for the treated group. The IS/OS predicted trend line between the groups had comparable slopes. (Grey dots represent individual mouse data points. Black lines connect the mean outcome at each time point. Red lines are estimated mean trend lines from linear regression models, assuming linearity of the outcome over time. Dashed lines are used for controls, and solid lines are used for knockout mice. Comparisons of *Tsc1*$^{-/-}$*Pde6b*$^{H620Q/H620Q}$ versus *Tsc1*$^{loxP/loxP}$*Pde6b*$^{H620Q/H620Q}$ at fixed points: ONL nuclei density: Week 4 $P < 0.001$, Week 5 $P = 0.10$, Week 6 $P = 0.03$, Week 8 $P = 0.75$, Week 10 $P = 0.33$; ONL width: Week 4 $P < 0.001$, Week 5 $P = 0.06$, Week 6 $P = 0.002$, Week 8 $P = 0.49$, Week 10 $P = 0.27$; IS/OS width: Week 4 $P = 0.002$, Week 5 $P = 0.02$, Week 6 $P < 0.001$, Week 8 $P = 0.65$, Week 10 $P = 0.12$. Comparison of the slopes between the two groups from the linear regression models: ONL density $P = 0.06$, ONL width $P = 0.05$, IS/OS $P = 0.39$. First n value represents *Tsc1*$^{-/-}$*Pde6b*$^{H620Q/H620Q}$, and second n represents *Tsc1*$^{loxP/loxP}$*Pde6b*$^{H620Q/H620Q}$: Week 4 $n = 9$ and $n = 6$, Week 5 $n = 5$ and $n = 4$, Week 6 $n = 9$ and $n = 4$, Week 8 $n = 4$ and $n = 6$, Week 10 $n = 5$ and $n = 6$.).

other retinal cells, as the whole retina was harvested for analysis (Fig. 7B). Conversely, mTOR, p-mTOR and their downstream targets were upregulated in the knockout mice, including pS6, glucose transporter 1 (GLUT1) and phosphorylated 4E binding protein-1 (p4EBP1), which promotes protein synthesis (25,26). Conversely, no difference in expression was found in unphosphorylated S6 and 4EBP1 in the *Tsc1*$^{loxP/loxP}$*Pde6b*$^{H620Q/H620Q}$ versus the *Tsc1*$^{-/-}$*Pde6b*$^{H620Q/H620Q}$ mice. Sterol regulatory element binding protein-1 (SREBP1) is another downstream target of mTOR that stimulates lipogenesis (27), although no significant difference was detected between two groups. Autophagy protein 5 (ATG5), a primary autophagy protein regulated by the

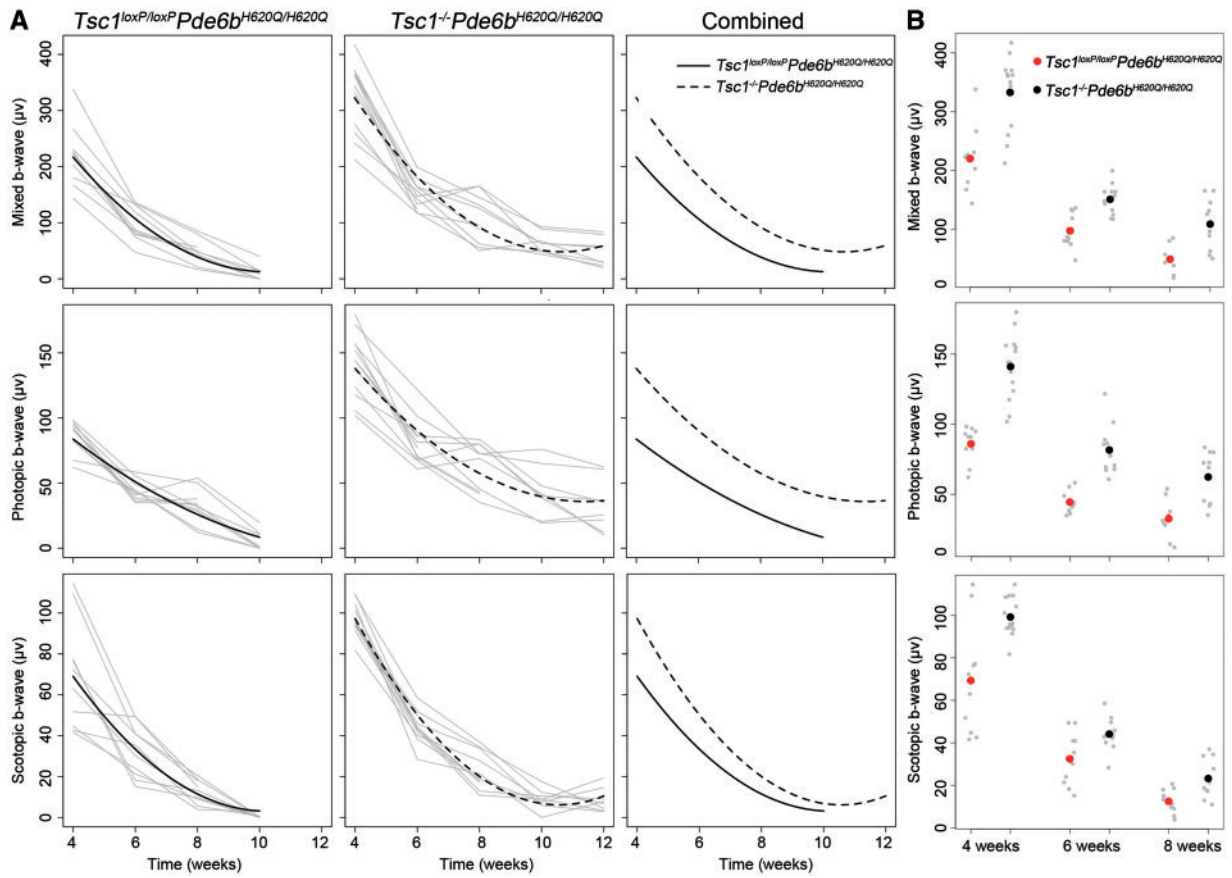

Figure 4. Retinal function was statistically improved in *Tsc1*$^{-/-}$*Pde6b*$^{H620Q/H620Q}$ mice compared to controls. **(A)** ERG scotopic, photopic, and mixed b-wave amplitudes were acquired over time, and mean b-wave responses were higher in *Tsc1*$^{-/-}$*Pde6b*$^{H620Q/H620Q}$ mice compared with controls. (Grey lines are eyes from individual mice. From the linear mixed models, solid black lines are estimated mean trajectories for the controls, and dashed black lines are for the experimental group. Likelihood ratio tests: Scotopic $P < 0.001$, Mixed $P = 0.002$, Photopic $P = 0.01$. Week 4 both groups $n = 6$, Week 6 $n = 6$ for *Tsc1*$^{-/-}$*Pde6b*$^{H620Q/H620Q}$ $n = 5$ for *Tsc1*$^{loxP/loxP}$*Pde6b*$^{H620Q/H620Q}$, Week 8 both groups $n = 5$, Week 10 both groups $n = 4$, Week 12 $n = 4$ for *Tsc1*$^{-/-}$*Pde6b*$^{H620Q/H620Q}$, $n = 0$ for *Tsc1*$^{loxP/loxP}$*Pde6b*$^{H620Q/H620Q}$). **(B)** Comparisons of knockout versus control mice at fixed points revealed that mean b-wave recordings were higher at every time point in the *Tsc1*$^{-/-}$*Pde6b*$^{H620Q/H620Q}$ group compared to controls and were statistically significant at each time point. (Small grey dots represent data points from individual eyes; bold red dots represent means for the *Tsc1*$^{loxP/loxP}$*Pde6b*$^{H620Q/H620Q}$, while bold black dots represent means for *Tsc1*$^{-/-}$*Pde6b*$^{H620Q/H620Q}$. Scotopic: Week 4 $P = 0.02$, Week 6 $P = 0.08$, Week 8 $P = 0.04$. Mixed: Week 4 $P = 0.003$, Week 6 $P = 0.003$, Week 8 $P = 0.01$. Photopic: Week 4 $P < 0.001$, Week 6 $P = 0.001$, Week 8 $P = 0.02$).

mTOR pathway, was also assessed, but again, no statistical difference was detected between groups. GLUT1, which increases glucose uptake into cells (28), was shown to be upregulated in the experimental group. Changes in protein fold were quantified and revealed that the greatest difference between the groups was in mTOR, p-mTOR, p4EBP1, pS6 and GLUT1 levels, all of which were increased in the knockout mice.

Safety data for *Tsc1*$^{-/-}$*Pde6b*$^{H620Q/H620Q}$ mice: no tumour formation

Tsc1$^{-/-}$*Pde6b*$^{H620Q/H620Q}$ mice were observed for 16 months (Fig. 8), and then eight organs were dissected for H&E staining. Sections from the heart, brain, lungs and other major organs did not show any signs of tumour formation.

Discussion

In this paper, we demonstrated that both rod and cone degeneration can be rescued in the early stages by ablating the *Tsc1* gene specifically in rods. We used morphological assays to determine these results and, to our knowledge, are the first to provide electrophysiology data to demonstrate that restoring balance towards anabolism can be therapeutic. This finding builds off the work of groups like Punzo et al., who found metabolic aberrations in the insulin/mTOR signalling pathway in the cones of four different mouse models of RP. Systemic treatment with insulin encouraged cone survival, suggesting that there may be a metabolic basis to retinal degeneration in these models (21,29). Our paper advances these findings by corroborating their cone results in rods and identifying a potential mechanism to explain how mTOR upregulation promotes anabolism. Notably, we demonstrate that enhancing the mTOR pathway in rods can also promote cone cell survival. This may be due to rod-derived nutritional factors that are required to sustain cones, and thus, promoting rod survival may enhance the release of such factors and concurrently increase preservation of cones (30–32). In a study of rod-cone dystrophy, heightened rod-derived cone viability factor (RdCVF) expression led to cone preservation for up to 5 weeks (33). In comparison, our study achieved cone rescue for up to 20 weeks and rod rescue up to 12 weeks. For therapeutic purposes, either early treatment of rods or simultaneous treatment of rods and cones together may afford the greatest possibility of achieving retinal survival.

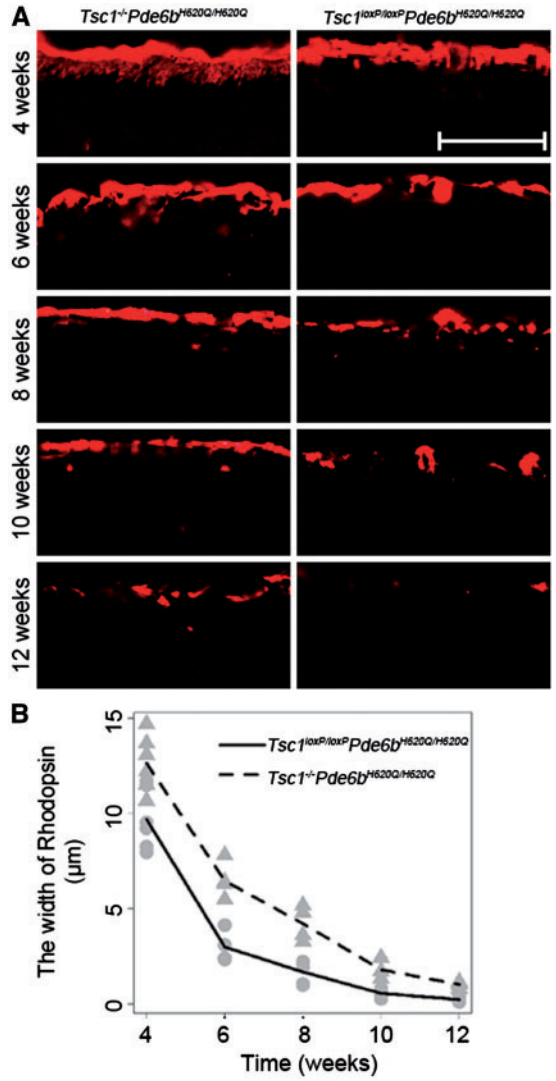

Figure 5. RHO immunoreactivity reveals rod preservation over 12 weeks in $Tsc1^{-/-}Pde6b^{H620Q/H620Q}$ mice. **(A)** Immunofluorescence staining of RHO was more intense in the IS/OS layer of $Tsc1^{-/-}Pde6b^{H620Q/H620Q}$ mice compared to controls at every time point. (Scale bar = 20 μm.) **(B)** The width of RHO-expression in the IS/OS was measured at 300 microns from the optic nerve and quantified. A statistically greater mean width in the experimental group compared to controls was found at every time point. (Grey circles represent data from individual control mice; grey triangles represent individual experimental mice. The solid black line connects means for controls, and the dashed black line represents means for the experimental group. Week 4 $P = 0.008$, Week 6 $P < 0.001$, Week 8 $P = 0.005$, Week 10 $P = 0.006$, Week 12 $P < 0.001$. Week 4 $n = 6$ for both groups, Week 6 $n = 4$ for $Tsc1^{-/-}Pde6b^{H620Q/H620Q}$, $n = 5$ for $Tsc1^{loxP/loxP}Pde6b^{H620Q/H620Q}$, Week 8 $n = 5$ for $Tsc1^{-/-}Pde6b^{H620Q/H620Q}$, $n = 4$ for $Tsc1^{loxP/loxP}Pde6b^{H620Q/H620Q}$, Weeks 10 and 12 $n = 4$ for both groups.).

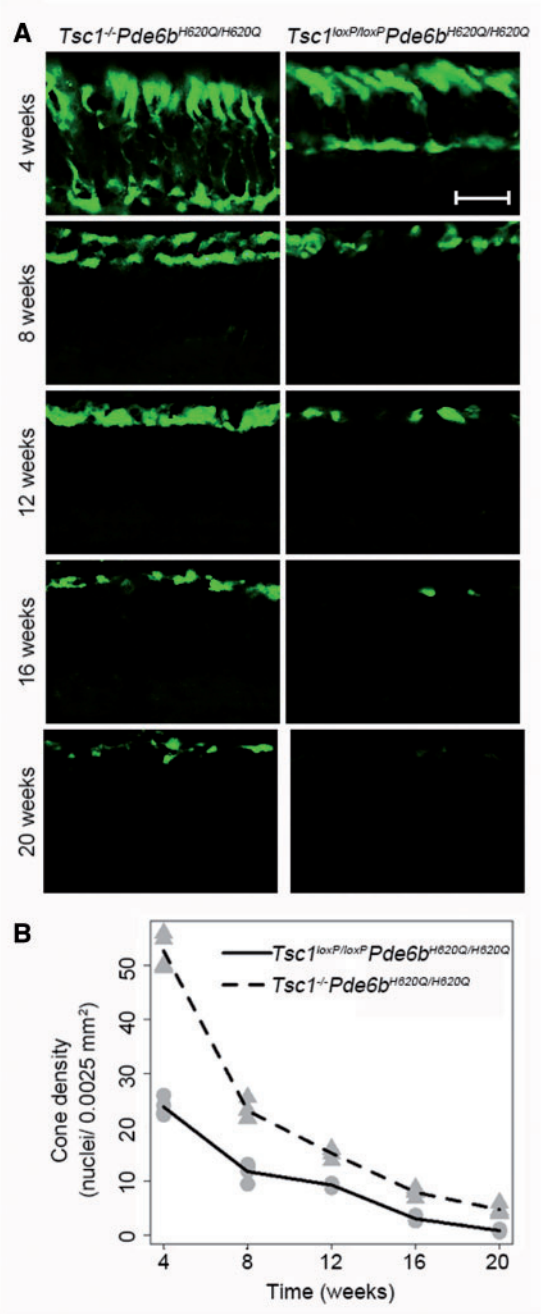

Figure 6. Cone arrestin immunoreactivity reveals suggests cone preservation over time in $Tsc1^{-/-}Pde6b^{H620Q/H620Q}$ mice. **(A)** Cones were stained with anti-cone arrestin antibody at multiple time points. Higher mean anti-cone arrestin immunoreactivity was observed in the $Tsc1^{-/-}Pde6b^{H620Q/H620Q}$ mice, compared to controls at every time point. In both groups, there was a decline in staining over time. (Scale bar = 20 μm.). **(B)** Photoreceptor nuclei numbers were quantified, and a statistically significant higher mean density was observed for the experimental group at every time point. (Grey circles represent data from individual mice from the control group; grey triangles represent individual mice from the experimental group. The solid black line represents means for controls, and the dashed black line represents means for the experimental group. For all-time points, $n = 4$ for both groups, and $P < 0.001$, except Week 20, where $P = 0.002$.

Several notable results can be garnered from our data. First, in the early stages of degeneration, TSC1 deficiency is effective at retarding degeneration in the ONL (Fig. 2). While both the experimental and control groups experienced decreases in the ONL over time, the rate of degeneration was slower for the experimental group. Surprisingly, the reverse was true in the late stages of degeneration, where the rate of degeneration was faster in the experimental group than in the control group. This may indicate that at later time points, rescue is harder to achieve, and perhaps upregulation of mTOR is not sufficient to stave off culminated Ca^{2+}/cyclic guanosine monophosphate (cGMP) toxicity caused by the $Pde6b^{H620Q/H620Q}$ mutation (22).

Another notable finding is that the width of the IS/OS layers actually increased during the early stages of degeneration in

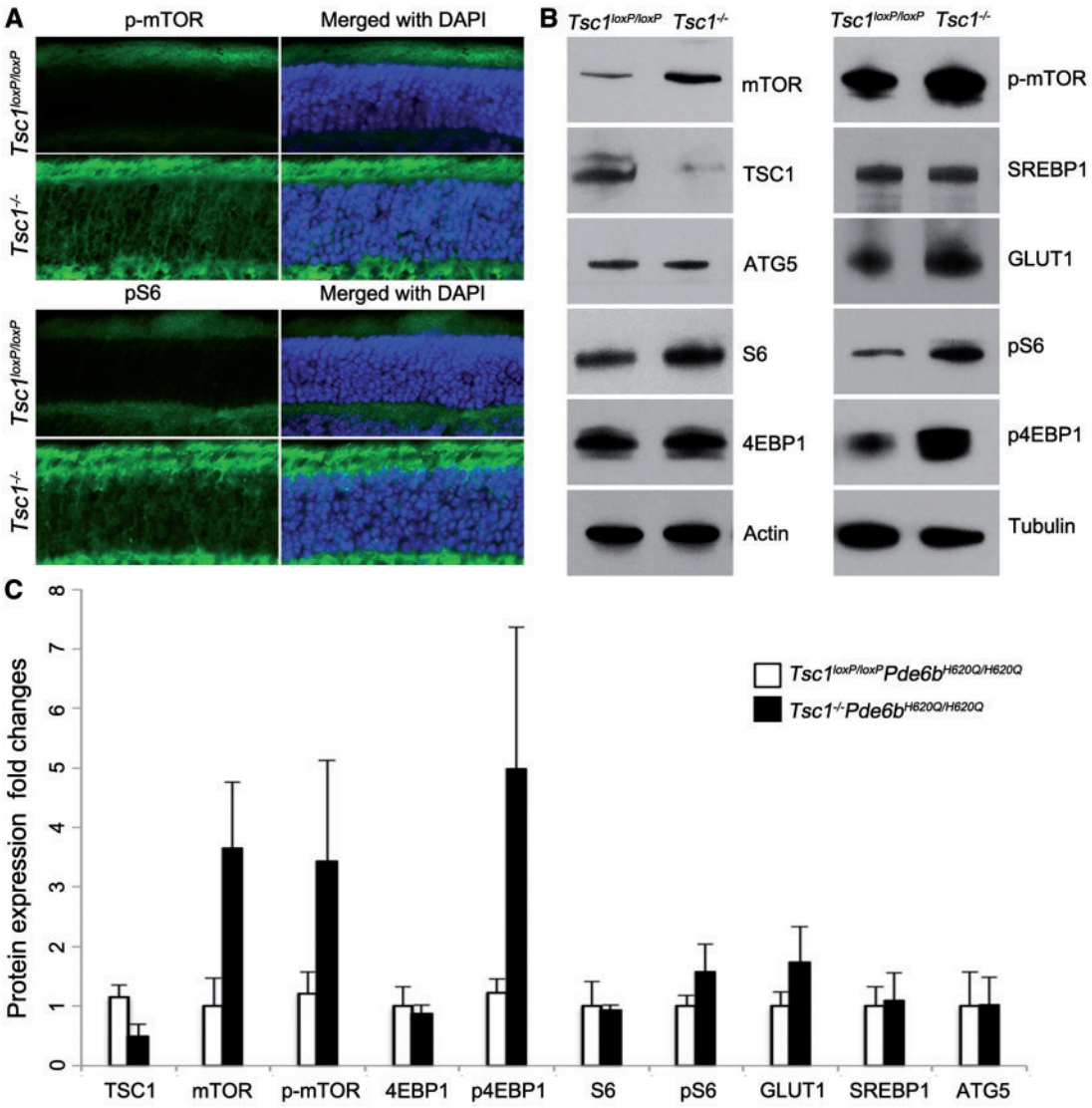

Figure 7. Downstream targets of mTOR are upregulated in $Tsc1^{-/-}Pde6b^{H620Q/H620Q}$ mice. **(A)** Increased expression of phosphorylated mTOR and the downstream protein S6 was detected in immunofluorescence staining in the IS/OS layers as well as the ONL in the experimental mice. Merged DAPI images of nuclei revealed the location of the ONL. (Scale bar = 20 μm.) **(B)** Immunoblot revealed upregulated mTOR, p-mTOR, pS6, GLUT1, and p4EBP1 expression levels and downregulated TSC1 levels in the experimental versus control groups. S6, 4EBP1, SREBP1, and ATG5 expression levels were not significantly affected by *Tsc1* ablation. Actin and tubulin served as loading controls. **(C)** Protein expression was quantified by analysing the fold change between the control and experimental groups. There was a statistically significant increase in mean protein expression in mTOR, p-mTOR, p4EBP1, pS6, and GLUT1, and a significant decrease in mean expression in TSC1 in the experimental group compared to the controls. (TSC1 $P < 0.05$, mTOR $P < 0.05$, p-mTOR $P < 0.05$, 4EBP1 $P = 0.49$, p4EBP1 $P < 0.05$, S6 $P = 0.78$, pS6 $P < 0.05$, SREBP $P = 0.76$, ATG5 $P = 0.95$. $n = 4$ for both groups.).

both groups, although the slope of increase was higher in the $Tsc1^{-/-}Pde6b^{H620Q/H620Q}$ mice than in the controls. Unexpectedly, maintenance of IS/OS genesis occurred despite the ongoing ONL degeneration. At later time points, however, the IS/OS layer width began to decrease over time, and although the slopes of the groups were comparable, the $Tsc1^{-/-}Pde6b^{H620Q/H620Q}$ mouse still maintained a greater width at all-time points compared to $Tsc1^{loxP/loxP}Pde6b^{H620Q/H620Q}$ mice. These data suggest that perhaps TSC1 deficiency enhances IS/OS biogenesis during early periods of development, or it may slow the rate of IS/OS degeneration. An alternative explanation for the slowed photoreceptor dysgenesis could be that TSC1 deficiency in rods improved retinal development as opposed to retarding degeneration. Further studies must be undertaken to distinguish which of these hypotheses most accurately reflects the physiology of the rescue.

Our data also demonstrated that TSC1 ablation upregulated the downstream targets of the mTOR pathway, namely pS6, p4EBP1 and GLUT1. While the former two effectors – pS6 and p4EBP1 – stimulate protein synthesis, the lattermost – GLUT1 – regulates glucose transport (28). Specifically, GLUT1 increases glucose uptake into cells, and its upregulation may be indicative of increased metabolism. Thus, upregulation of anabolic processes such as protein and lipid synthesis in OS may have retarded the cell death signals. This is supported by previous studies. GLUT1 has been shown to play a pivotal role in cone protection by TSC2 ablation, which enhanced the mTOR pathway (29). Additionally, GLUT1 is an essential component for rod

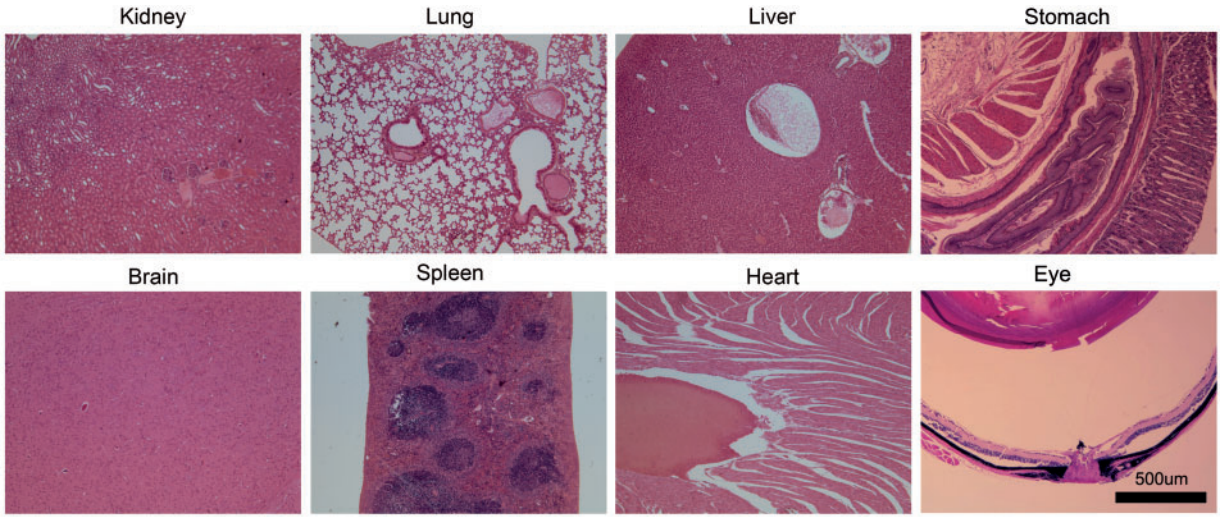

Figure 8. No tumour formation up to 16 months following Tsc1 ablation in *Pde6b*$^{H620Q/H620Q}$ mice. *Tsc1*$^{-/-}$*Pde6b*$^{H620Q/H620Q}$ mice were observed for sixteen months. Major organs were subsequently harvested and subjected to H&E staining, which did not reveal tumour formations in any tested organs ($n = 5$).

protection via activity of rod-derived cone viability factor (30). Notably, ATG5 expression did not vary between control and experimental mice. ATG5 is a main autophagy protein regulated by the mTOR pathway. Studies have shown that this protein supports colour vision and the preservation of phototransduction in rods. Furthermore, deletion of *ATG5* in wild type mice was shown to induce retinal degeneration (34,35). However, our findings seem to suggest that the deleterious effects may operate through another mechanism other than ATG5. Our data instead align more closely with the theory that upregulation of anabolic processes could be a potential non-gene-specific therapy for patients with retinal degeneration.

While enhancing the mTOR pathway could be a potential risk for tumour formation, safety data acquired from knockout mice over 16 months indicates that *TSC1* ablation does not lead to tumour formation, likely because the Cre driver is highly specific to rods and does not target other organs. Our study also shows that early treatment is more effective at slowing the rate of degeneration. From our previous studies on the mTOR pathway, we found that similar results can be achieved by silencing *Tsc2*, and perhaps the combination of knocking out *Tsc1* and *Tsc2* simultaneously may hold the most potential for abrogating the degeneration that is characteristic of this disease. Additional future studies exploring this strategy would be beneficial to elucidating the mechanistic connection between the upregulated effectors of anabolism and the slowed neurodegeneration observed.

The genetic heterogeneity of RP poses limitations to monotherapy, i.e. gene-specific treatment. Currently, four gene therapy trials for an early-onset form of RP are ongoing (36–39). Although these trials initially demonstrated some functional improvement, such gene-specific trials are costly. With more than 60 genes implicated in the development of RP, this is an impractical strategy that is not amenable to large-scale production or treatment. We have demonstrated here that promoting anabolic pathways in rods can improve their resistance to degeneration in a non-gene-specific manner. Recent research from other groups supports the important role of metabolism, not only in retinal degeneration, but also in neural degenerative conditions in general (40–43). Reprogramming a terminally differentiated neuron to remain in an anabolic state is applicable to a diverse range of genetic deficits and could potentially be used to treat multiple neurodegenerative conditions. The mTOR pathway is highly druggable, and appears to be a ubiquitous self-defence mechanism in many types of cell pathways. Targeting the mTOR pathway is, at the least, a starting point for the development of non-gene-specific therapeutics.

Materials and Methods

Animals

The Columbia University Institutional Animal Care and Use Committee (IACUC) approved all experiments prior to study initiation, and mice were used in accordance with the Statement for the Use of Animals in Ophthalmic and Vision Research of the Association for Research in Vision and Ophthalmology and the Policy for the Use of Animals in Neuroscience Research of the Society for Neuroscience.

Three lines of mice were crossed to generate the control and experimental mice. *Ped6b*^{H620Q}/*Pde6b*^{H620Q} mice were rederived via oviduct transfer using the European Mouse Mutant Archive (EMMA) morulae (22,44); *Pde6g*^{CreERT2} mice were generated in the Barbara & Donald Jonas Stem Cell & Regenerative Medicine Laboratory (45–51); and *Tsc1*^{tm1Djk}*/J* were purchased from the Jackson Laboratory (Stock No. 005680) (52). All mice were housed in the Columbia University Pathogen-free Eye Institute Annex Animal Care Services Facility and maintained with a 12-h light/12-h dark cycle.

Pde6b^{H620Q}/*Pde6b*^{H620Q} and *Pde6g*^{CreERT2} mice were crossed; their offspring were then bred with *Tsc1*^{tm1Djk}*/J* mice. Four generations of backcrosses yielded heterozygous *Tsc1*$^{-/-}$ *Pde6b*$^{H620Q/+}$*Pde6g*^{CreERT2} mice (Fig. 1), and six generations of backcrosses yielded homozygous *Tsc1*$^{-/-}$*Pde6b*$^{H620Q/H620Q}$*Pde6g*^{CreERT2} mice (all other figures).

At P7, half of the mice from each group injected at P7, 9 and 11 with 100 μg/g body weight of tamoxifen (100 mg/ml in ethanol; catalog T5648; Sigma-Aldrich), which was diluted with corn oil to a concentration of 10 mg/ml and mixed thoroughly at 42 °C. The rest of the mice were injected in an identical fashion with ethanol (10% in corn oil) instead of tamoxifen. The former served as the experimental group and the latter, the control

group. No discrimination based on the sex of the mice was made in regards to group assignment.

Immunoblotting

Using a previously published method (46,48), retinae were collected from 3-week-old mice and subsequently homogenized in M-PER Mammalian Protein Extraction Reagent (Prod #78501 Thermo Scientific), which was supplemented with phosphatase inhibitor cocktail 1 (catalog P2850-5 ml; Sigma) and protease inhibitor cocktail (catalog P8340-1 ml; Sigma). The bicinchoninic acid (BCA) protein assay (Thermo Scientific) was used to measure protein concentrations, and sodium dodecyl sulphate–polyacrylamide gel electrophoresis (SDS-PAGE; 4%–15%; Bio-Rad) was used to separate proteins. Samples were then transferred to nitrocellulose (Bio-Rad), blocked in 5% skim milk (902887 MP Biomedicals, LLC), then incubated overnight at 4 °C in the following antibodies: Hamartin/TSC1 Antibody (Cell Signaling Technology,4906), Anti-mTOR Antibody (Cell Signaling Technology,2972), Anti-mTOR (phospho S2448) antibody (Abcam,ab109268), Anti-S6 Ribosomal Protein (Cell Signaling Technology,2217) Antibody, Phospho-S6 Ribosomal Protein (Ser240/244) (Cell Signaling Technology,5364S) Antibody, Anti-4E-BP1 (Cell Signaling Technology,53H11) Antibody, Phospho-4E-BP1 (Ser65) (174A9) mAb (Cell Signaling Technology,9456), SREBP1 (2A4) (ThermoFisher,MA5-16124) Antibody, Anti-APG5L/ATG5 (Abcam,ab109490) Antibody, Anti-Glucose Transporter GLUT1 (Abcam,40084) Antibody, α-Tubulin Antibody (Cell Signaling Technology,2144S) Antibody, and Anti-beta Actin (Abcam,125248) Antibody. After washing three times in 0.5% PBST (500 µl Tween-20 in 1,000 ml PBS), they were then incubated for 1 h at room temperature with goat anti-rabbit IgG-HRP secondary antibody (1:2,000; catalog sc-2004; Santa Cruz Biotechnology, Inc.) or rabbit anti-mouse IgG-HRP sc-358914 HRP conjugated antibody (1:2,000; sc-358914; Santa Cruz Biotechnology Inc.). Chemiluminescent detection (EMD Millipore) using Biomax film (Kodak) revealed membrane proteins. We then measured the level of a particular protein in $Tsc1^{-/-}Pdeb6^{H620Q/H620Q}$ and $Tsc1^{loxP/loxp}Pde6b^{H620Q/H620Q}$ mice ($n=4$ for each group). Image J analysis software was used to analyse bands. Protein levels were normalized respective to tubulin levels. Levels from one of the $Tsc1^{loxP/loxp}Pde6b^{H620Q/H620Q}$ mice were normalized to 1, and all other experimental conditions were compared to this. A *t*-test was used to compare the statistical difference between the two groups.

ONL density and inner/outer segment length measurement

The cornea and lens were dissected and the vitreous removed from enucleated eyes to isolate the eyecup following mouse euthanasia, performed following established IACUC guidelines and previously described procedures (46,48). H&E and retinal paraffin sections were prepared at 5 µm in size using excalibur pathology, and then they were divided into four regions: peripheral temporal; central temporal; central nasal; and peripheral nasal regions. Photoreceptor nuclei in each region were quantified using Image J (NIH, Bethesda). The ONL thickness was also measured in each of the four quadrants and averaged; the IS/OS length was ascertained in the same manner.

Immunohistochemistry

Eyes were enucleated and submerged in 4% paraformaldehyde for 1 h at room temperature. Retinae were then dissected from the eyecup, cryoprotected using 30% glucose overnight at 4 °C, then sectioned vertically at 10 µm with a cryostat (Leica). After washing 3 times with phosphate-buffered saline (PBS, pH 7.4), sections were incubated overnight at 4 °C with the following primary antibodies: rabbit anti-cone arrestin (1:5000, Millipore), mouse anti-rhodopsin (1:500, Santa Cruz Biotechnology),Anti-mTOR (phospho S2448) antibody (Abcam,ab109268),Phospho-S6 Ribosomal Protein (Ser235/236) Antibody(Cell Signaling Technology,9456) diluted in 5% Chemiblocker (Life Technologies) and 0.3% Triton X-100 in PBS. The sections were subsequently washed in PBS, then incubated with secondary antibodies conjugated to either Alexa 555 or Alexa 488 (1:500, Molecular Probes, Life Technologies) for 1 h at room temperature. Sections were washed again with PBS, then incubated for 5 min with 5 µg/ml Hoechst 33342 (Molecular Probes). The sections were analysed by microscopy (Leica), and only those containing the optic nerve were included for analysis. Five sections were analysed and averaged for each mouse. The RHO's width was measured at 300 µm from the optic nerve of both sides by Image J(NIH,Bethesda).The average of five slices of each mouse were analysed to represent each mouse.Using the same method cone nuclei density was quantified manually.

ERG

The mice were dark-adapted overnight. Mice were then anaesthetized by way of intraperitoneal injection using 1 ml of 100 mg/ml ketamine and 0.1 ml of 20 mg/ml xylazine in 8.9 ml PBS at a concentration of 0.1 ml /10g BW and placed on heating pads to maintain a 37 °C body temperature. One drop of tropacamide ophthalmic solution (1%, Akorn) was delivered to dilate each, and 10 min later, electrodes were placed on the conreas and Gonisol Hypromellose Ophthalmic Demulcent Solution (2.5%, Akron) was administered. ERG recordings were subsequently recorded under dim red light illumination. Both eyes were simultaneously recorded using the Electrophysiological system (Diagnosys). Pulses of 0.00130 cd/m^2 and 3 cd/m^2 (White-6500K) were used to collect rod and maximal rod and cone ERG responses, with 40 to 60 trials per result. To assess the cone response, mice were light-adapted in the Ganzfeld dome for 10 min, then exposed to white flashes while ERGs were recorded. A background of 30 cd/m^2 (White-6500K) light was used throughout the trial to suppress rod responses. ERGs were recorded at 4, 6, 8, 10 and 12 weeks.

Statistics

For $Tsc1^{-/-}Pde6b^{H620Q/+}$ and $Tsc1^{loxP/loxP}Pde6b^{H620Q/+}$ mice, to compare differences in mean ERG or histology outcome levels between the two groups, linear mixed models were fitted with random intercepts for mouse, since we have two observations per mouse.

For the H&E staining histological analysis in the retinal degeneration background, we only have one observation per mouse. To compare histology outcomes between groups at a fixed time point, *t*-tests were used to compare means. To compare the change in histology outcomes over time between groups, linear regression models were fit, where the predictors were group, time, and a group by time interaction.

For the ERG analysis in the retinal degeneration background, we have two observations per mouse at each time point. To compare ERG outcomes between groups at a fixed time point, linear mixed models with random intercepts for mouse were fit.

To compare the trajectory of ERG outcomes over time between groups, linear mixed models with random intercepts for mouse were fit, where the predictors were group, time, time-squared and interactions between group and time variables. To test whether mean trajectories were different between groups, likelihood ratio tests were used.

We also compared mean differences between groups for the following outcomes: rhodopsin, anti-cone arrestin and mTOR pathway protein expression levels. For these, we have one observation per mouse, and so, means were compared using *t*-tests.

Study approval

The IACUC of Columbia University approved animal experiments before initiation of the project, and mice were used in accordance with the Statement for the Use of Animals in Ophthalmic and Vision Research of the Association for Research in Vision and Ophthalmology, and the Policy for the Use of Animals in Neuroscience Research of the Society for Neuroscience.

Acknowledgements

We would like to thank members of the Jonas Stem Cell Laboratory and the Brown Glaucoma Laboratory for sharing ideas and equipment.

Conflict of Interest statement. None declared.

Funding

This work was conducted in the Barbara & Donald Jonas Laboratory of Regenerative Medicine and Bernard & Shirlee Brown Glaucoma Laboratory, which are supported by the CDMRP TSCRP:TS080017, National Institute of Health [5P30EY019007, R01EY018213, R01EY024698, 1R01EY026682, R21AG050437]; National Cancer Institute Core [5P30CA013696]; the Research to Prevent Blindness (RPB) Physician-Scientist Award; unrestricted funds from RPB, New York, NY, USA; the Tistou and Charlotte Kerstan Foundation; the Crowley Family Fund; the Schneeweiss Stem Cell Fund; New York State [C029572]; the Foundation Fighting Blindness New York Regional Research Center Grant [C-NY05-0705-0312]; and the Gebroe Family Foundation. JY is supported by National Natural Science Funds [81400412], China and the Key Program of Tianjin Natural Science Foundation [15JCZDJC34500] Tianjin, China. VBM is supported by NIH grants [K08EY020530, R01EY024665, R01EY025225, R01EY024698 and R21AG050437] and RPB. AGB is supported by 1R01NS098590-01.

References

1. Hartong, D.T., Berson, E.L. and Dryja, T.P. (2006) Retinitis pigmentosa. *Lancet*, **368**, 1795–1809.
2. Hamel, C. (2006) Retinitis pigmentosa. *Otphanet J. Rare Dis.*, **1**, 40.
3. Fahim, A.T., Daiger, S.P. and Weleber, R.G. (1993) Pagon, R.A., Adam, M.P., Ardinger, H.H., Wallace, S.E., Amemiya, A., Bean, L.J.H., Bird, T.D., Fong, C.T., Mefford, H.C., Smith, R.J.H. and Stephens, K. (eds.), In *GeneReviews(R)*, Seattle (WA), in press.
4. Lin, M.K., Tsai, Y.T. and Tsang, S.H. (2015) Emerging treatments for retinitis pigmentosa: Genes and stem cells, as well as new electronic and medical therapies, are gaining ground. *Retin Physician*, **12**, 52–70.
5. Daiger, S.P., Bowne, S.J. and Sullivan, L.S. (2007) Perspective on genes and mutations causing retinitis pigmentosa. *Arch. Ophthalmol.*, **125**, 151–158.
6. Daiger, S.P., Sullivan, L.S., Gire, A.I., Birch, D.G., Heckenlively, J.R. and Bowne, S.J. (2008) Mutations in known genes account for 58% of autosomal dominant retinitis pigmentosa (adRP). *Adv. Exp. Med. Biol.*, **613**, 203–209.
7. Sullivan, L.S., Bowne, S.J., Birch, D.G., Hughbanks-Wheaton, D., Heckenlively, J.R., Lewis, R.A., Garcia, C.A., Ruiz, R.S., Blanton, S.H., Northrup, H., *et al.* (2006) Prevalence of disease-causing mutations in families with autosomal dominant retinitis pigmentosa: a screen of known genes in 200 families. *Invest. Ophthalmol. Vis. Sci.*, **47**, 3052–3064.
8. Friedman, D.S., O'Colmain, B.J., Munoz, B., Tomany, S.C., McCarty, C., de Jong, P.T., Nemesure, B., Mitchell, P., Kempen, J. and Eye Diseases Prevalence Research, G. (2004) Prevalence of age-related macular degeneration in the United States. *Arch. Ophthalmol.*, **122**, 564–572.
9. Molday, R.S. and Moritz, O.L. (2015) Photoreceptors at a glance. *J. Cell Sci.*, **128**, 4039–4045.
10. Punzo, C., Xiong, W. and Cepko, C.L. (2012) Loss of daylight vision in retinal degeneration: are oxidative stress and metabolic dysregulation to blame? *J. Biol. Chem.*, **287**, 1642–1648.
11. Kurihara, T., Westenskow, P.D., Gantner, M.L., Usui, Y., Schultz, A., Bravo, S., Aguilar, E., Wittgrove, C., Friedlander, M., Paris, L.P., *et al.* (2016) Hypoxia-induced metabolic stress in retinal pigment epithelial cells is sufficient to induce photoreceptor degeneration. *Elife*, **5**, 5. pii: e14319.
12. Veleri, S., Lazar, C.H., Chang, B., Sieving, P.A., Banin, E. and Swaroop, A. (2015) Biology and therapy of inherited retinal degenerative disease: insights from mouse models. *Dis. Model Mech.*, **8**, 109–129.
13. Liko, D. and Hall, M.N. (2015) mTOR in health and in sickness. *J. Mol. Med. (Berl)*, **93**, 1061–1073.
14. Martinez de Morentin, P.B., Martinez-Sanchez, N., Roa, J., Ferno, J., Nogueiras, R., Tena-Sempere, M., Dieguez, C. and Lopez, M. (2014) Hypothalamic mTOR: the rookie energy sensor. *Curr. Mol. Med.*, **14**, 3–21.
15. Howell, J.J., Ricoult, S.J., Ben-Sahra, I. and Manning, B.D. (2013) A growing role for mTOR in promoting anabolic metabolism. *Biochem. Soc. Trans.*, **41**, 906–912.
16. Proud, C.G. (2006) Regulation of protein synthesis by insulin. *Biochem. Soc. Trans.*, **34**, 213–216.
17. Astrinidis, A. and Henske, E.P. (2005) Tuberous sclerosis complex: linking growth and energy signaling pathways with human disease. *Oncogene*, **24**, 7475–7481.
18. Xue, H., Ji, Y., Wei, S., Yu, Y., Yan, X., Liu, S., Zhang, M., Yao, F., Lan, X. and Chen, L. (2016) HGSD attenuates neuronal apoptosis through enhancing neuronal autophagy in the brain of diabetic mice: the role of AMP-activated protein kinase. *Life Sci.*, **153**:23–34.
19. Evangelisti, C., Cenni, V. and Lattanzi, G. (2016) Potential therapeutic effects of the mTOR inhibitors for preventing ageing and progeria-related disorders. *Br. J. Clin. Pharmacol.*, **82**, 1229–1244.
20. Tsang, S.H., Chan, L., Tsai, Y.T., Wu, W.H., Hsu, C.W., Yang, J., Tosi, J., Wert, K.J., Davis, R.J. and Mahajan, V.B. (2014) Silencing of tuberin enhances photoreceptor survival and function in a preclinical model of retinitis pigmentosa (an american ophthalmological society thesis). *Trans. Am. Ophthalmol. Soc.*, **112**, 103–115.

21. Punzo, C., Kornacker, K. and Cepko, C.L. (2009) Stimulation of the insulin/mTOR pathway delays cone death in a mouse model of retinitis pigmentosa. *Nat. Neurosci.*, **12**, 44–52.
22. Davis, R.J., Tosi, J., Janisch, K.M., Kasanuki, J.M., Wang, N.K., Kong, J., Tsui, I., Cilluffo, M., Woodruff, M.L., Fain, G.L., *et al.* (2008) Functional rescue of degenerating photoreceptors in mice homozygous for a hypomorphic cGMP phosphodiesterase 6 b allele (Pde6bH620Q). *Invest. Ophthalmol. Vis. Sci.*, **49**, 5067–5076.
23. Kurumaji, Y. and Miyazaki, K. (1990) Tiopronin-induced lichenoid eruption in a patient with liver disease and positive patch test reaction to drugs with sulfhydryl group. *J. Dermatol.*, **17**, 176–181.
24. Olney, J.W. (1968) An electron microscopic study of synapse formation, receptor outer segment development, and other aspects of developing mouse retina. *Invest. Ophthalmol.*, **7**, 250–268.
25. Dickinson, J. (1990) Sharing the pain of motherhood. *Nurs. Times*, **86**, 36–38.
26. Gardner, T.W., Abcouwer, S.F., Losiewicz, M.K. and Fort, P.E. (2015) Phosphatase control of 4E-BP1 phosphorylation state is central for glycolytic regulation of retinal protein synthesis. *Am. J. Physiol. Endocrinol. Metab.*, **309**, E546–E556.
27. Griffiths, B., Lewis, C.A., Bensaad, K., Ros, S., Zhang, Q., Ferber, E.C., Konisti, S., Peck, B., Miess, H., East, P., *et al.* (2013) Sterol regulatory element binding protein-dependent regulation of lipid synthesis supports cell survival and tumor growth. *Cancer Metab.*, **1**, 3.
28. Caron, A., Richard, D. and Laplante, M. (2015) The roles of mTOR complexes in lipid metabolism. *Annu. Rev. Nutr.*, **35**, 321–348.
29. Venkatesh, A., Ma, S., Le, Y.Z., Hall, M.N., Ruegg, M.A. and Punzo, C. (2015) Activated mTORC1 promotes long-term cone survival in retinitis pigmentosa mice. *J. Clin. Invest.*, **125**, 1446–1458.
30. Ait-Ali, N., Fridlich, R., Millet-Puel, G., Clerin, E., Delalande, F., Jaillard, C., Blond, F., Perrocheau, L., Reichman, S., Byrne, L.C., *et al.* (2015) Rod-derived cone viability factor promotes cone survival by stimulating aerobic glycolysis. *Cell*, **161**, 817–832.
31. Sahel, J.A., Mohand-Said, S., Leveillard, T., Hicks, D., Picaud, S. and Dreyfus, H. (2001) Rod-cone interdependence: implications for therapy of photoreceptor cell diseases. *Prog. Brain Res.*, **131**, 649–661.
32. Mohand-Said, S., Hicks, D., Dreyfus, H. and Sahel, J.A. (2000) Selective transplantation of rods delays cone loss in a retinitis pigmentosa model. *Arch. Ophthalmol.*, **118**, 807–811.
33. Byrne, L.C., Dalkara, D., Luna, G., Fisher, S.K., Clerin, E., Sahel, J.A., Leveillard, T. and Flannery, J.G. (2015) Viral-mediated RdCVF and RdCVFL expression protects cone and rod photoreceptors in retinal degeneration. *J. Clin. Invest.*, **125**, 105–116.
34. Zhou, Z., Doggett, T.A., Sene, A., Apte, R.S. and Ferguson, T.A. (2015) Autophagy supports survival and phototransduction protein levels in rod photoreceptors. *Cell Death Differ.*, **22**, 488–498.
35. Zhou, Z., Vinberg, F., Schottler, F., Doggett, T.A., Kefalov, V.J. and Ferguson, T.A. (2015) Autophagy supports color vision. *Autophagy*, **11**, 1821–1832.
36. Maguire, A.M., High, K.A., Auricchio, A., Wright, J.F., Pierce, E.A., Testa, F., Mingozzi, F., Bennicelli, J.L., Ying, G.S., Rossi, S., *et al.* (2009) Age-dependent effects of RPE65 gene therapy for Leber's congenital amaurosis: a phase 1 dose-escalation trial. *Lancet*, **374**, 1597–1605.
37. Lopes, V.S. and Williams, D.S. (2015) Gene therapy for the retinal degeneration of usher syndrome caused by mutations in MYO7A. *Cold Spring Harb. Perspect. Med.*, **5**,
38. Ghazi, N.G., Abboud, E.B., Nowilaty, S.R., Alkuraya, H., Alhommadi, A., Cai, H., Hou, R., Deng, W.T., Boye, S.L., Almaghamsi, A., *et al.* (2016) Treatment of retinitis pigmentosa due to MERTK mutations by ocular subretinal injection of adeno-associated virus gene vector: results of a phase I trial. *Hum. Genet.*, **135**, 327–343.
39. Kousal, B., Dudakova, L., Hlavata, L. and Liskova, P. (2016) Clinical tests testing new therapies for stargardt disease. *Cesk. Slov. Oftalmol.*, **72**, 293–297.
40. Du, J., Rountree, A., Cleghorn, W.M., Contreras, L., Lindsay, K.J., Sadilek, M., Gu, H., Djukovic, D., Raftery, D., Satrustegui, J., *et al.* (2016) Phototransduction influences metabolic flux and nucleotide metabolism in mouse retina. *J. Biol. Chem.*, **291**, 4698–4710.
41. Cepko, C. and Punzo, C. (2015) Cell metabolism: Sugar for sight. *Nature*, **522**, 428–429.
42. Demetrius, L.A. and Driver, J. (2013) Alzheimer's as a metabolic disease. *Biogerontology*, **14**, 641–649.
43. Demetrius, L.A. and Simon, D.K. (2012) An inverse-Warburg effect and the origin of Alzheimer's disease. *Biogerontology*, **13**, 583–594.
44. Hart, A.W., McKie, L., Morgan, J.E., Gautier, P., West, K., Jackson, I.J. and Cross, S.H. (2005) Genotype-phenotype correlation of mouse pde6b mutations. *Invest Ophthalmol. Vis. Sci.*, **46**, 3443–3450.
45. Koch, S.F., Tsai, Y.T., Duong, J.K., Wu, W.H., Hsu, C.W., Wu, W.P., Bonet-Ponce, L., Lin, C.S. and Tsang, S.H. (2015) Halting progressive neurodegeneration in advanced retinitis pigmentosa. *J. Clin. Invest.*, **125**, 3704–3713.
46. Tsang, S.H., Gouras, P., Yamashita, C.K., Kjeldbye, H., Fisher, J., Farber, D.B. and Goff, S.P. (1996) Retinal degeneration in mice lacking the gamma subunit of the rod cGMP phosphodiesterase. *Science*, **272**, 1026–1029.
47. Tsang, S.H., Chen, J., Kjeldbye, H., Li, W.S., Simon, M.I., Gouras, P. and Goff, S.P. (1997) Retarding photoreceptor degeneration in Pdegtm1/Pdegtml mice by an apoptosis suppressor gene. *Invest. Ophthalmol. Vis. Sci.*, **38**, 943–950.
48. Tsang, S.H., Burns, M.E., Calvert, P.D., Gouras, P., Baylor, D.A., Goff, S.P. and Arshavsky, V.Y. (1998) Role for the target enzyme in deactivation of photoreceptor G protein in vivo. *Science*, **282**, 117–121.
49. Tanabe, T., Tsang, S.H., Kjeldbye, H., Berns, K., Goff, S. and Gouras, P. (1998) Adeno-associated virus mediated gene transfer into PDE g knockout mouse. *Invest. Ophthalmol. Vis. Sci.*, S5153. in press.,
50. Tosi, J., Sancho-Pelluz, J., Davis, R.J., Hsu, C.W., Wolpert, K.V., Sengillo, J.D., Lin, C.S.S. and Tsang, S.H. (2011) Lentivirus-mediated expression of cDNA and shRNA slows degeneration in retinitis pigmentosa. *Exp. Biol. Med. (Maywood, N.J.)*, **236**, 1211–1217.
51. Tsang, S.H., Tsui, I., Chou, C.L., Zernant, J., Haamer, E., Iranmanesh, R., Tosi, J. and Allikmets, R. (2008) A novel mutation and phenotypes in phosphodiesterase 6 deficiency. *Am. J. Ophthalmol.*, **146**, 780–788.
52. Kwiatkowski, D.J., Zhang, H., Bandura, J.L., Heiberger, K.M., Glogauer, M., el-Hashemite, N. and Onda, H. (2002) A mouse model of TSC1 reveals sex-dependent lethality from liver hemangiomas, and up-regulation of p70S6 kinase activity in Tsc1 null cells. *Hum. Mol. Genet.*, **11**, 525–534.